Aircraft Observations and Numerical Simulations of the Developing Stage of a Southerly Surge near Southern California

THOMAS R. PARISH

Department of Atmospheric Science, University of Wyoming, Laramie, Wyoming

DAVID A. RAHN

Department of Geography and Atmospheric Science, University of Kansas, Lawrence, Kansas

DAVE LEON

Department of Atmospheric Science, University of Wyoming, Laramie, Wyoming

(Manuscript received 6 November 2014, in final form 18 September 2015)

ABSTRACT

Summertime low-level winds in the marine boundary layer off the California coast are predominantly from the north. This pattern is interrupted periodically by southerly winds and low stratus that can propagate for hundreds of kilometers northward along the coast. These events have been termed coastally trapped disturbances, coastally trapped wind reversals, and southerly surges; their forcing has been the subject of extensive study and debate. Southerly surges remain difficult to forecast, yet have a significant impact on coastal activities.

The beginning stage of a southerly surge on 16 June 2012 was explored during the Precision Atmospheric Marine Boundary Layer Experiment. Measurements of the horizontal wind and pressure field in the marine layer offshore from Cape Arguello hours prior to the onset of the surge were made using the University of Wyoming King Air research aircraft. Airborne measurements show that a horizontal pressure field is established with higher pressure to the south just prior to the surge, supporting southerly ageostrophic winds and a south-to-north movement of marine stratus. Aircraft soundings and lidar returns confirm the existence of offshore flow of warm, continental air north of Point Arguello that alters the pressure field adjacent to the coast. The southerly surge originates near Point Arguello and propagates northward past San Francisco during the early morning hours on 17 June 2012. Results from the Weather Research and Forecasting Model are consistent with the King Air observations. Analyses and model output presented here confirm that the large-scale environment is critical to the initiation of these wind reversals.

1. Introduction

Winds in the summertime atmospheric marine boundary layer (MBL) off the California coast (see Fig. 1 for a map of key geographical features and station locations) develop as a result of the horizontal pressure field set up by the Pacific high situated several hundred kilometers to the west of the coast and the thermal low over the desert southwest. Subsidence above the Pacific high establishes a temperature inversion at the top of the well-mixed MBL. Observations have shown that the depth of the MBL increases to the west with the largest changes near the coast (e.g., Beardsley et al. 1987; Pomeroy and Parish 2001). Coastal jets are often observed in the MBL as a response. Time-averaged isobars run approximately parallel to the coastline within the MBL and north winds persist for most of the summer. Numerous authors have documented the characteristics of the flow in the MBL through observations (e.g., Beardsley et al. 1987; Zemba and Friehe 1987; Mass and Albright 1987; Parish 2000; Pomeroy and Parish 2001; Rahn and Parish 2007) and numerical simulations (e.g., Burk and Thompson 1996; Koračin and Dorman 2001; Rahn and Parish 2007; Hsu et al. 2007).

The northerly summer MBL wind regime near the coast is interrupted periodically by episodes of southerly winds that are usually accompanied by coastal stratus or fog.

Corresponding author address: Thomas R. Parish, Department of Atmospheric Science, University of Wyoming, Laramie, WY 82071.
E-mail: parish@uwyo.edu

DOI: 10.1175/MWR-D-15-0140.1

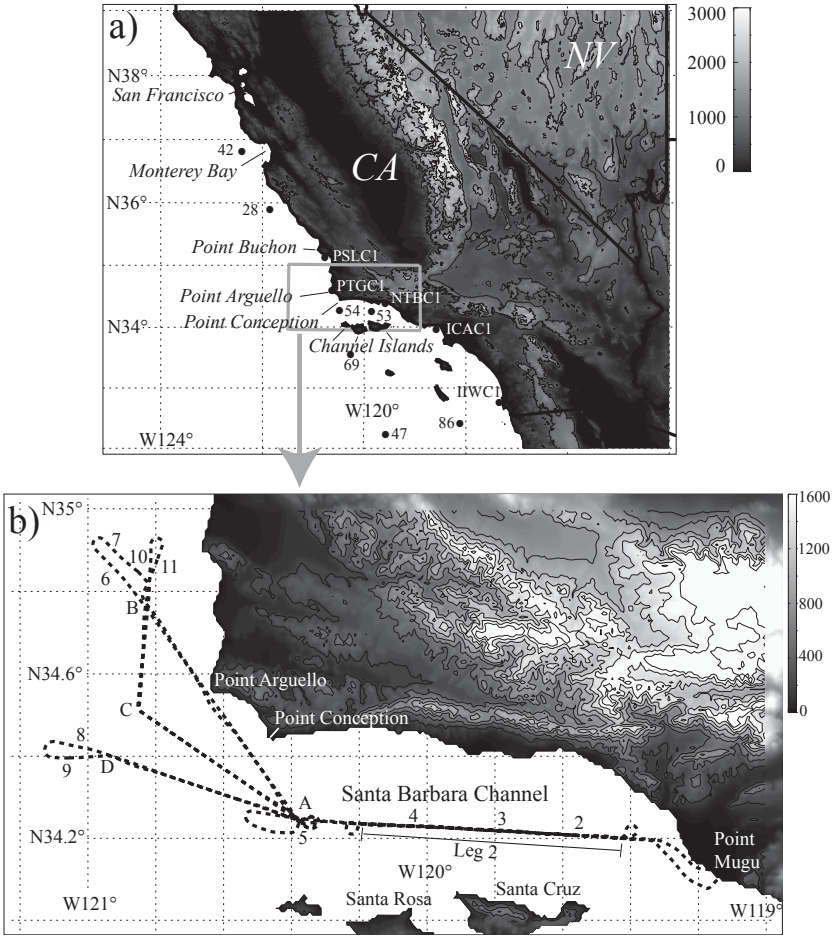

FIG. 1. Terrain elevation (m) (a) along the California coast showing key surface stations, buoys (No. 460xx), and geographical features, and (b) a close-up of Santa Barbara Channel region showing the PreAMBLE flight track on 16 Jun 2012 (bold dashed line). The letters and numbers along track indicate reference locations for flight legs and soundings discussed in the text. Approximate times that the aircraft passes by each point are as follows: A at 1805, 1850, 1922, and 2003 UTC; B at 1827 and 1945 UTC; C at 1838 and 1935 UTC; and D at 1906 UTC.

These wind reversals, also known as coastally trapped wind reversals, coastally trapped disturbances, or southerly surges, develop adjacent to the coastline. The offshore extent of a southerly surge is on the order of 100 km. They often propagate northward for hundreds of kilometers along the coast (e.g., Ralph et al. 1998; Parish et al. 2008).

Southerly surges have been the topic of extensive study. Dorman (1985) noted that southerly surges had characteristics similar to Kelvin waves and proposed that the northward progression was forced by perturbations in the MBL height along the coastal topography that acts as the rigid lateral boundary. Mass and Albright (1987) offered an alternate explanation, suggesting that they result from alongshore horizontal pressure gradients created by synoptic conditions. The resulting flow of a wind reversal is simply an ageostrophic downgradient response. Bond et al. (1996) and Mass and Bond (1996) examined the climatology and synoptic-scale circulations associated with southerly surges. They noted that for strong cases a pattern emerges that consists of offshore-directed flow near 850 hPa over California.

Subsiding flow over the coastal mountains and associated adiabatic warming and offshore warm advection leads to a significant lowering of pressure in the near-coastal environment. Higher surface pressures are observed to the south and, thus, the alongshore horizontal pressure gradient becomes reversed. A discussion of key issues and a summary of wind reversal studies can be found in Nuss et al. (2000).

A major limitation in resolving the competing interpretations of southerly surges has been the lack of observations within the wind reversal environment. Few in situ airborne measurements of the wind reversal environment have been obtained. The 10–11 June 1994

event, perhaps the most studied wind reversal to date (e.g., Ralph et al. 1998, 2000), was monitored by the University of North Carolina Piper Seneca III (Bane 1997; Nuss et al. 2000). Wind reversals were also captured during the 1996 Coastal Waves Experiment (Rogers et al. 1998), including the event of 21–22 July 1996 that is described in Nuss et al. (2000). More recently, Parish et al. (2008) and Rahn and Parish (2008) described the 22–25 June 2006 case using data collected on board the University of Wyoming King Air in combination with and high-resolution numerical modeling.

Considerable progress has been made in understanding the forcing of wind reversals and the MBL structure associated with such events (e.g., Nuss 2007). Forecasts of surges have improved considerably during the past decade yet the timing and point of initiation of the developing stages of a wind reversal remain particularly difficult. While initiation can occur anywhere along the coast, events often commence near Point Arguello. An easterly flow over the region is associated with a greater offshore component to the north of the point than to the south. Thus, to the north there would be a greater drop in surface pressure and thinning of the MBL depth through offshore warm air advection and leeside subsidence that would promote a northward alongshore pressure gradient force. Another factor that can play a role is the presence of a Catalina eddy that is normally confined to the California Bight area, but that can also contribute to the initial surge and the ability of a particular event to ''break out'' from the bight remains a challenging forecast problem.

This paper presents aircraft observations and a numerical simulation of the initiation of a southerly surge along the Southern California coast near Point Arguello. The aircraft mission was part of the Precision Atmospheric Marine Boundary Layer Experiment (PreAMBLE) in May–June 2012. The primary goal of PreAMBLE was to study the atmospheric dynamics associated with the summertime MBL near the Point Arguello/Point Conception complex using the University of Wyoming King Air. A southerly surge developed during the evening of 16 June 2012 that progressed northward overnight and throughout the following day. Airborne observations were used to document the horizontal pressure field and the MBL structure at the inception of the wind reversal. Numerical simulation of the initiation of the southerly surge on 16–17 June 2012 was performed using the Weather Research and Forecasting (WRF) Model. Results are presented that supplement the aircraft observations.

2. Analysis of the large-scale environment

Satellite imagery at various stages of the wind reversal is shown in Fig. 2. At 2000 UTC 16 June 2012 (Fig. 2a), a 100-km-wide tongue of cloud just west of the Santa Barbara Channel is propagating toward the northeast. Farther west, however, the flow remains northerly. Three hours later (Fig. 2b) the tongue of cloud has impinged on the Southern California coastline north of Point Arguello. The wind reversal begins its northward surge along the coast during the evening hours (Fig. 2c). Surge stratus move about 350 km between 0200 and 1400 UTC; this corresponds to a propagation speed of about $8\,m\,s^{-1}$. Based on the classification in Bond et al. (1996) this surge easily classifies as ''strong'' ($\geq 5\,m\,s^{-1}$). The stratus moves past San Francisco, California, overnight (Fig. 2d). During the daytime hours on 17 June 2012, the surge reaches as far north as Point Arena where it stalls. Throughout the period, the northerly wind regime remains intact several hundred kilometers west of the shoreline.

As with other southerly surge cases (e.g., Thompson et al. 1997; Mass and Steenburgh 2000; Rahn and Parish 2010), preconditioning of the large-scale environment took place in the days preceding the initiation of the event. Figure 3 illustrates the sequence of 0000 UTC upper air analyses of isobaric heights, temperatures, and pressures at 500, 850, and 950 hPa, respectively, for 15–17 June 2012 from the 12-km horizontal resolution National Centers for Environmental Prediction North American Mesoscale Forecast System (NAM). At upper levels as indicated by the 500-hPa surface, a broad trough was positioned over Southern California at 0000 UTC 15 June. During the next 24 h, the trough became cut off from the main circulation. A relatively deep low developed that was centered west of the Baja Peninsula by 0000 UTC 17 June. In addition, 500-hPa ridging is apparent at this time into Northern and central California. As a consequence of this 0000 UTC 17 June 500-hPa height pattern, a well-organized offshore flow at 500 hPa existed across most of central and Southern California.

The 850-hPa height field shows similar features to those displayed on the 500-hPa maps. Ridging is apparent into the Pacific Northwest throughout the period and the broad thermal trough becomes displaced to the south. By 0000 UTC 17 June, 850-hPa heights also suggest considerable offshore flow across central and Southern California. Note that the temperature field clearly shows the effects of the offshore transport of warm, continental air west of the California coastline over a broad area.

The sequence of 0000 UTC maps from 15–17 June 2012 at the 950-hPa level illustrates the extension of the ridge into the Pacific Northwest. The strengthening of the offshore flow by 0000 UTC 17 June is evident. Strong warm air advection is present off the California coast

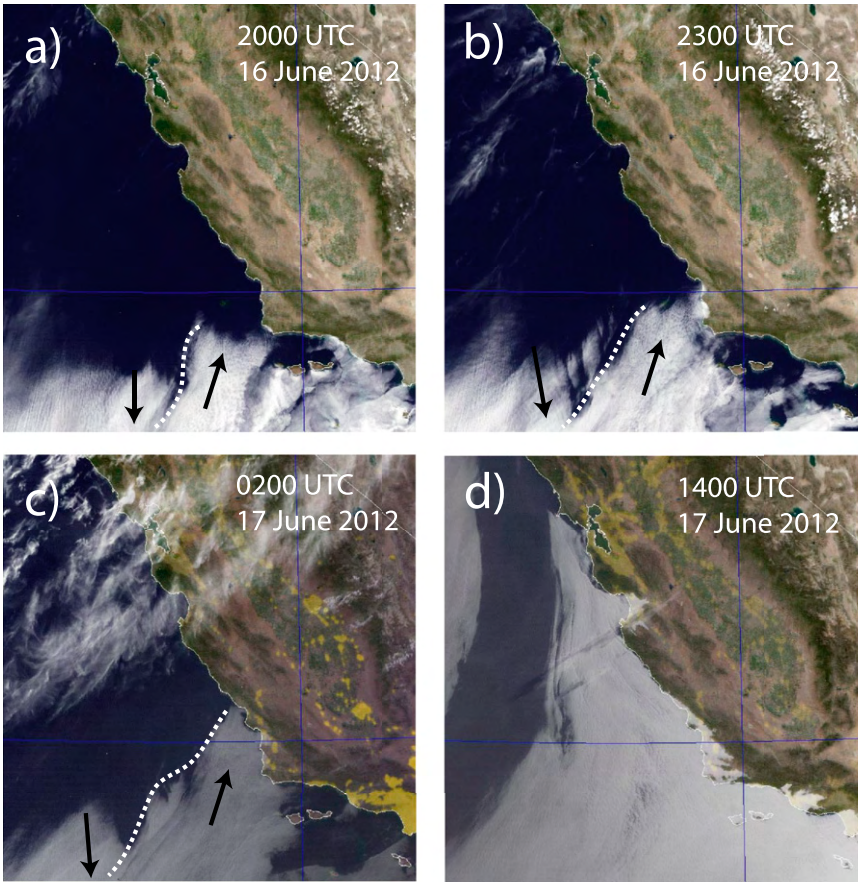

FIG. 2. GOES-West visible imagery at (a) 2000 UTC 16 Jun, (b) 2300 UTC 16 Jun, (c) 0200 UTC 17 Jun, and (d) 1400 UTC 17 Jun 2012. The black arrows indicated estimated wind directions based on cloud track motions; the white dashed lines indicate the estimated wind shift axis.

and the temperature field reveals temperatures near 30°C at 950 hPa west of San Francisco. Just prior to the initiation of the wind reversal early on 17 June, extensive offshore flow and warming is apparent throughout a relatively deep column of the atmosphere from 950 to 500 hPa.

Consequences of the offshore flow indicated in Fig. 3 on the dynamics of the near-surface airflow in the lowest levels of the atmosphere are profound. Replacement of cool, marine air with warm, continental air in the coastal environment is responsible for a significant decrease in pressure (e.g., Ralph et al. 1998). In addition, subsiding flow over the coastal mountains with associated adiabatic warming may enhance lee troughing in the near-coastal environment at low levels. The well-known Santa Ana wind events are an extreme case of strong downslope winds within the bight region south of Point Arguello that are associated with hot and dry conditions that create particularly dangerous fire conditions. From hydrostatic considerations, the warm column of air adjacent to the coastline results in lower pressure near the surface as compared to areas farther south (e.g., Mass and Bond 1996). Ralph et al. (1998), Mass and Steenburgh (2000), and Rahn and Parish (2008) have noted that a warming in the lowest 1–2 km of the atmosphere can lead to a local pressure decrease of up to 4 hPa, sufficient to reverse the alongshore pressure gradient force for the respective wind reversal cases.

Wind near the surface changes fairly rapidly over a short time as indicated by scatterometer data, buoy observations, and surface station observations (Fig. 4). Just prior to the King Air mission at 1735 UTC 16 June, winds near the shore south of Monterey Bay have already weakened and the westerly component has increased. Over the subsequent three hours the wind near Point Conception shifts and increases speed so that during the time of the King Air mission the wind is from the southwest at $\sim 6\,\mathrm{m\,s^{-1}}$, which is consistent with the lowest isobaric flights. A shift in the wind is evident over 100 km southwest of Point Conception. By

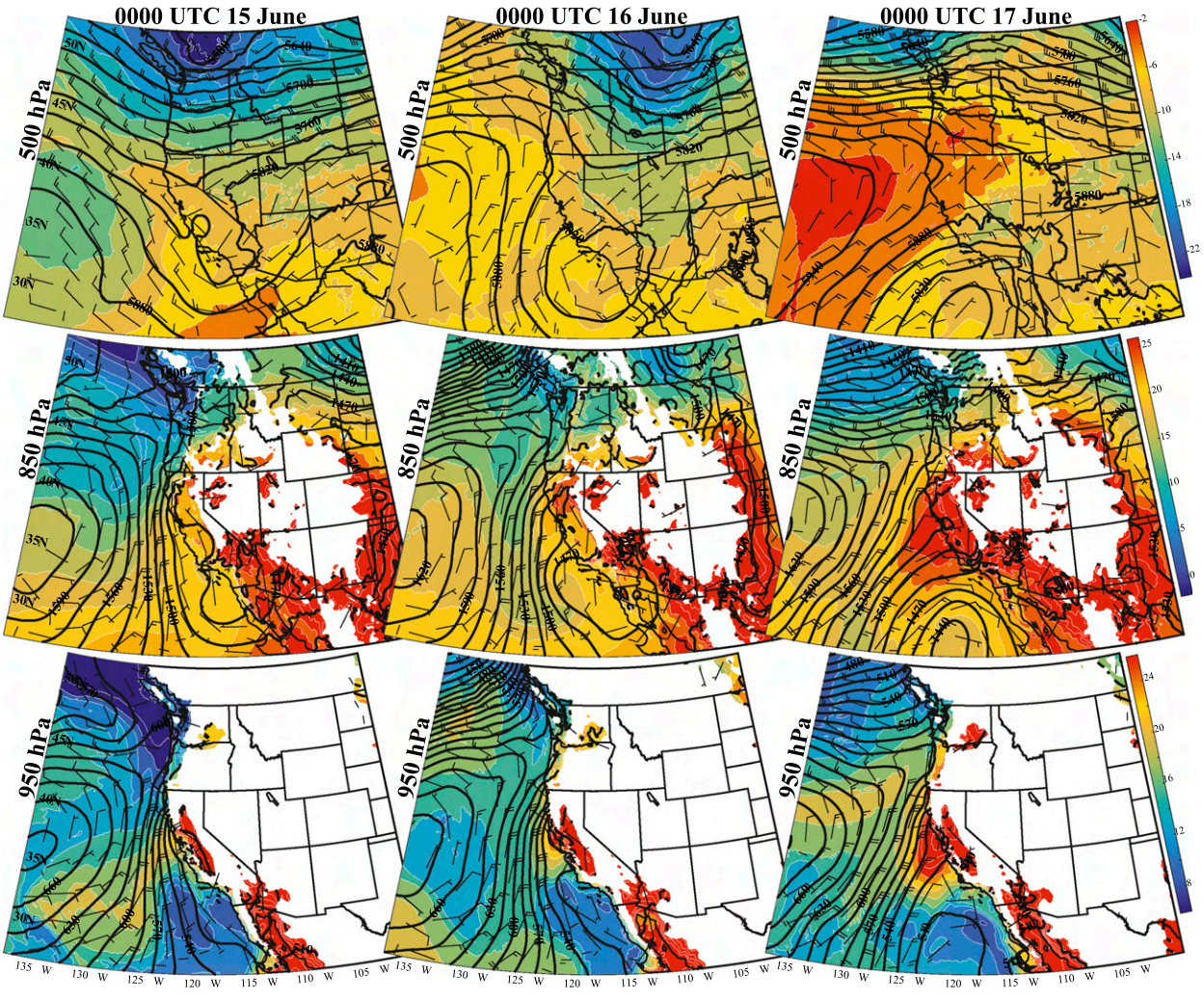

FIG. 3. The 0000 UTC (left) 15 Jun, (middle) 16 Jun, and (right) 17 Jun height contours (thick lines, m), wind barbs ($m\,s^{-1}$), and temperatures (color shaded, °C) at (top) 500, (middle) 850, and (bottom) 950 hPa. Data are from the NCEP NAM on the 218 grid (~12-km grid spacing).

0454 UTC 17 June it is clear that southerly wind encompasses a larger area and extends farther offshore. The southerly flow is just south of Monterey Bay by this time. Two hours later at 0735 UTC, the southerly wind is still nearing the bay. The edge of the low clouds can be approximated by the minimum in wind speed offshore between the southerly wind close to the shore and the northerly wind far offshore.

3. Airborne measurements of the environment prior to the southerly surge

a. Overview

The primary purpose of the King Air mission on 16 June 2012 was to map the horizontal pressure field within the MBL near Point Arguello when a wind reversal was likely to develop. A secondary purpose was to document conditions in the Santa Barbara Channel coincident with the formation of a southerly surge. The environment prior to the initiation of the wind reversal was sampled using the King Air from 1653 to 2034 UTC 16 June 2012.

Key instrumentation onboard the King Air included a reverse flow thermometer and a Rosemount 102 sensor to measure air temperature (accuracy 0.5°C), an Edge-Tech Vigilant model 137 to determine dewpoint temperature (accuracy 1°C), and a Rosemount 1501 High Accuracy Digital Sensing probe for static pressure (accuracy 0.5 hPa). Winds are determined from a Rosemount 858 five-hole gust probe mounted on the King Air (e.g., Lenschow et al. 1991) and have been corrected using the onboard GPS (accuracy $<1\,m\,s^{-1}$).

Precise measurements of the aircraft height above sea level while flying at a constant pressure level allows the horizontal pressure gradient to be determined (e.g.,

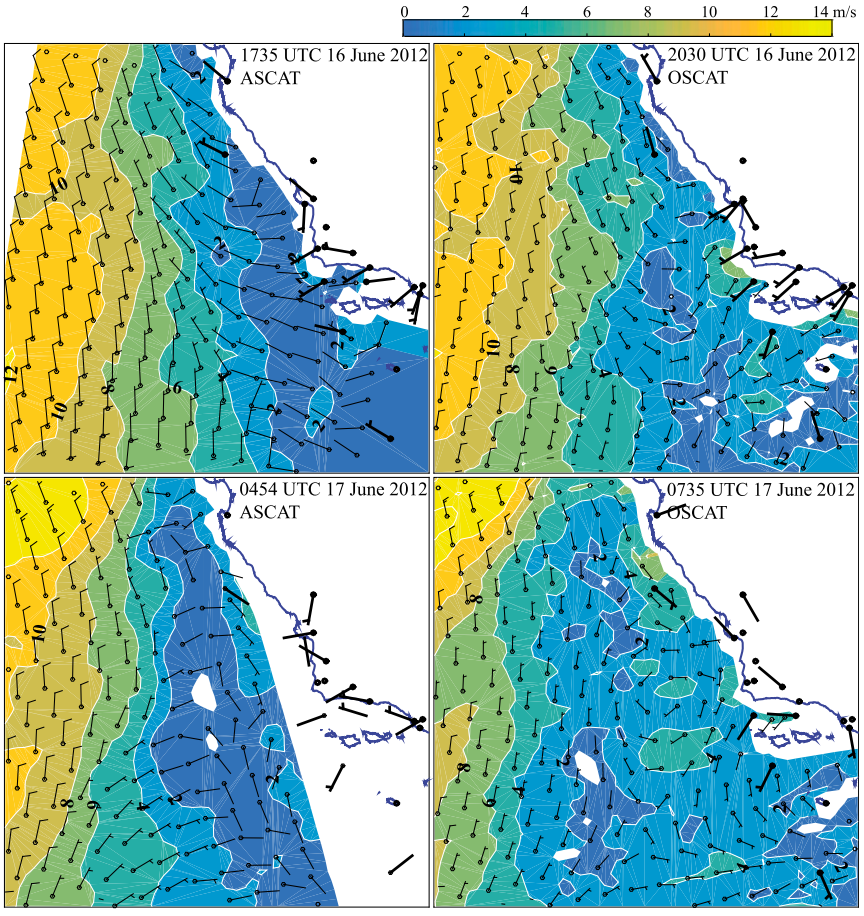

FIG. 4. Surface wind speed from the Advanced Scatterometer (ASCAT) and Oceansat Scatterometer (OSCAT) (color, m s^{-1}) and wind barbs (gray, m s^{-1}). Surface wind observations from buoy and surface stations closest to the time of the scatterometer overpass are indicated by the bold wind barbs.

Parish et al. 2007; Parish and Leon 2013). Two GPS receivers, an Ashtech Z-Sensor and a Trimble NetRS, are installed on the King Air and are used in the differential correction process to determine the three-dimensional position of the aircraft. Differential corrections were computed using the commercial package GrafNav 8.10 from NovAtel Inc.

The King Air also carried upward- and downward-looking versions of the Wyoming Cloud lidar (WCL). The upward- and downward-looking WCLs operate at 355 nm and are designed for retrieval of cloud and aerosol properties. Details regarding the lidars can be found in Wang et al. (2009) and Wang et al. (2012). The lidar data are combined with the inertial navigation system/GPS data from the King Air to produce time–height cross sections of the (uncalibrated) attenuated backscatter and the depolarization ratio (also uncalibrated). The lidars are well suited for determination of cloud boundaries and identification of the top of the boundary layer. However, clouds rapidly attenuate the lidar signal. Depolarization ratio, calculated from the ratio of the co- and cross-polarized returns, can be used to identify regions where nonspherical (i.e., dry) aerosol contributes significantly to the return. Low depolarization ratios are indicative of spherical or near-spherical particles, while high depolarization ratios are indicative of nonspherical particles. While higher depolarization ratios can indicate low humidity and effervesced aerosol, they more often correspond to nonhygroscopic aerosol (e.g., dust) and are indicative of air masses having a continental origin.

Complementing the lidar measurements, the King Air carried a Passive Cavity Aerosol Spectrometer Probe (PCASP). Aerosol greater than about 0.1 μm in diameter can be detected by this instrument (Cai et al. 2013) and size distributions from 0.1 to 3 μm can be determined.

The King Air took off at 1654 UTC 16 June 2012 heading west within the Santa Barbara Channel.

Satellite imagery (e.g., Fig. 2a) during the mission shows that clouds were present within the far eastern edge of the Santa Barbara Channel. Cyclonic circulation was evident in the California Bight on over two-thirds of the mornings during PreAMBLE. On this day, however, no cyclonic circulation was evident. Rather, satellite imagery showed the clouds to the south of the Channel Islands moving to the northwest throughout the day in an anticyclonic circulation. Initiation of some southerly surges has been linked to a ''break out'' of a strong Catalina eddy, but was not the case for this event.

After takeoff, the King Air climbed to about 1000 m, then descended to 115 m above the ocean and headed west within the Santa Barbara Channel. After traveling across the channel to just west of the Channel Islands, the King Air turned and headed back east along the same track. The purpose of the reciprocal legs was to measure the horizontal pressure gradient within the channel. After returning to the eastern part of the channel, the King Air turned again and headed west.

Mapping of the isobaric height field southwest of Point Conception used a ''spoke'' pattern (see Fig. 1), consisting of a series of isobaric legs about 115 m above the ocean adjacent to the Southern California coast. The first leg is roughly 100 km in length between points A and B in Fig. 1; soundings were conducted at the northwest end of the leg. The isobaric legs resumed with a 35-km track directly south between points B and C in Fig. 1 followed by a 60-km leg heading southeast between points C and A in Fig. 1, returning to the hub of the spoke pattern. The King Air then headed back west-northwest for a final 75-km leg between points A and D in Fig. 1. Soundings were conducted at the far western edge of the isobaric leg and the pattern was then repeated in reverse before the King Air headed back to the base at Point Mugu. Isallobaric effects can be determined since the aircraft repeatedly passes through the central ''hub.'' This allows a correction to the height measurements to ensure an accurate assessment of the horizontal pressure gradient force.

b. *Measurements within the Santa Barbara Channel*

King Air measurements for the second isobaric leg within the Santa Barbara Channel, conducted between 120.2° and 119.4°W (1728–1743 UTC; see Fig. 1b for leg 2 track), are shown in Fig. 5. Flight level was roughly 115 m above the ocean at a mean pressure of about 999 hPa. The King Air was below the cloud, thus the upward pointing lidar can measure cloud-base height (Fig. 5a). Clouds were present in the eastern half of the Santa Barbara Channel with cloud-base height increasing to the west.

Analysis of the height of the 999-hPa isobaric surface across the channel from the differential GPS processing (Fig. 5b) shows a horizontal pressure gradient with lower pressure to the west. The magnitude of the pressure gradient is small, amounting to about 0.2 hPa over 75 km. The direction of such a pressure field is anomalous. Measurements on other days during PreAMBLE (e.g., Parish et al. 2014) and mean summertime conditions (e.g., Dorman and Koračin 2008) show pressures that decrease from west to east within the channel.

Winds within the Santa Barbara Channel (Fig. 5c) are weak, averaging less than 3 m s^{-1}. The wind direction along the far eastern edge of the leg is primarily from the south. North of Santa Cruz Island, the easternmost of the Channel Islands, the wind direction becomes more easterly, perhaps in part due to the topographic influence of the islands. The western cloud boundary is aligned with the western edge of Santa Cruz Island. Wind direction shifts to the south-southwest at the western end of the leg.

Temperature and dewpoint temperature (Fig. 5d) at the 999-hPa level display little change along the leg. The western end of the leg is about 1 K cooler than the eastern end. Sea surface temperatures display an abrupt 2-K change across the cloud edge with colder temperatures associated with the cloud-free environment. Satellite imagery shows that the cloud thinned throughout the day and that the western edge of the cloud did not move westward past Santa Cruz Island despite the favorable horizontal pressure field. Both the 999-hPa wind speed and wind direction appear linked to the sea surface temperature. Winds decrease and turn from easterly to more southwesterly, coincident with the sea surface temperature decrease. Such changes may result from the topographic influences on both low-level atmospheric flows as well as sea surface temperatures.

c. *The horizontal pressure field adjacent to the coastline*

As with the isobaric leg in the Santa Barbara Channel, the flight level during the spoke pattern was set at 999 hPa. Clear skies prevailed during most of the mapping. The northern edge of the cloud tongue, shown in Fig. 3a, is just south of line AC in Fig. 1. By the second mapping pattern, the cloud layer was reaching legs AC and AD.

The resulting isobaric height field from the two mapping patterns (1809–1902 and 1910–2003 UTC) is illustrated in Fig. 6. Lowest isobaric heights are found closest to the coast just north of Point Arguello in each case with highest heights to the south. This height field is anomalous as compared to the mean isobaric height fields seen from other PreAMBLE cases (e.g., Parish et al. 2014; Rahn et al. 2014) in which lowest heights typically are found south of Point Conception. The

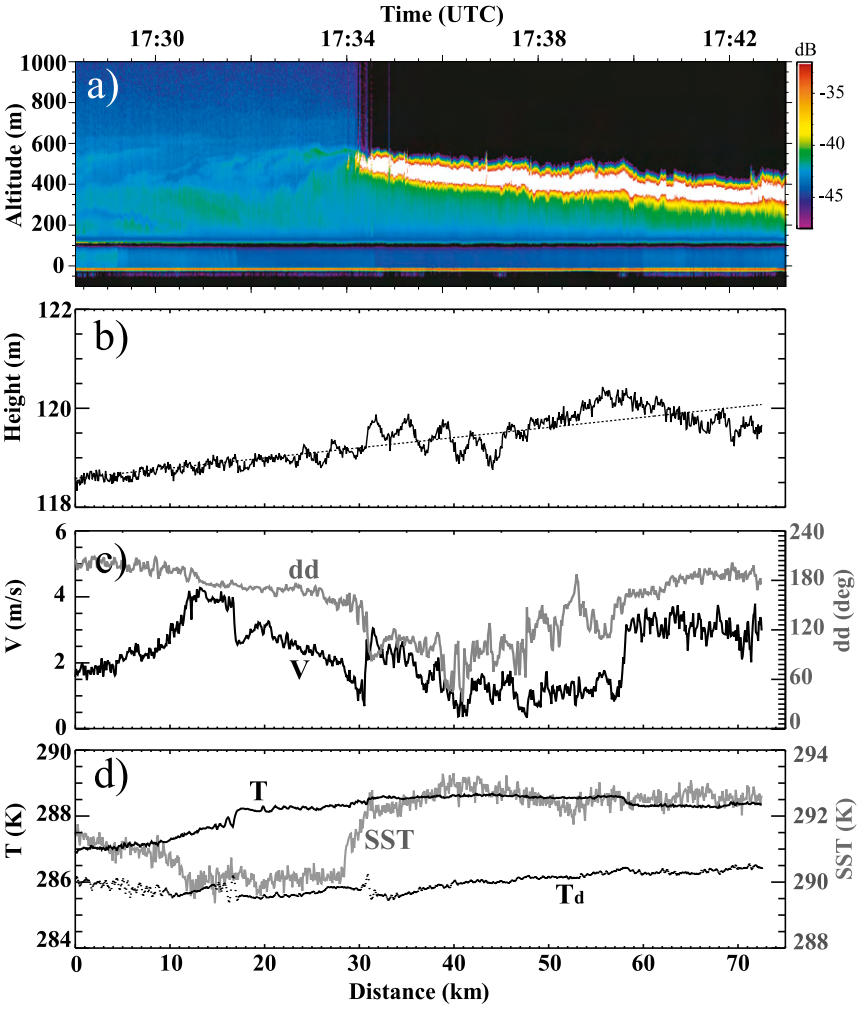

FIG. 5. King Air measurements from 999-hPa leg 2 (between 120.2° and 119.4°W) from 1728 to 1743 UTC 16 Jun 2012 of (a) lidar return from WCL (dB); (b) isobaric heights (bold line, m) with least squares linear fit (dashed line); (c) wind speeds (bold line, m s^{-1}) and wind direction (gray line, degrees, axis to right); and (d) temperature (bold, solid line, K), dewpoint temperature (dashed, K), and sea surface temperature (solid, gray line, K). West is to the left.

reversal of the pressure gradient force in the region with higher pressure to the south is essential for development of a southerly surge (e.g., Mass and Bond 1996).

The magnitude of this pressure gradient is significant. The maximum south–north isobaric height gradient shown in Figs. 6a and 6b is roughly 4 m over a distance of 20 km, corresponding to a horizontal pressure change of slightly less than 0.5 hPa $(20\,\text{km})^{-1}$. Winds at the 999-hPa level as shown in Fig. 6 are directed downgradient. Acceleration is apparent as wind speeds increase from south to north in response to the pressure field. Wind directions at flight level are predominantly from the south over the southern portion of the flight pattern but display a distinct clockwise turning north of Point Arguello, becoming directed toward the coastal terrain. Measured winds are consistent with the cloud motion in the area as evidenced by the satellite imagery (Fig. 2). We view this period in which the flow accelerates toward the coast north of Point Arguello as the beginning of the southerly surge.

Skamarock et al. (1999) conducted idealized numerical experiments and emphasized the importance of low pressure in the marine environment adjacent to the shoreline in the initiation of surge events. They hypothesize that the marine layer flows around the low are blocked by the coastal mountains, resulting in deepening of the marine layer. It is this elevated marine layer that moves northward as the surge, having characteristics of a Kelvin wave. The main features of a Kelvin wave include gradual perturbations of the MBL depth

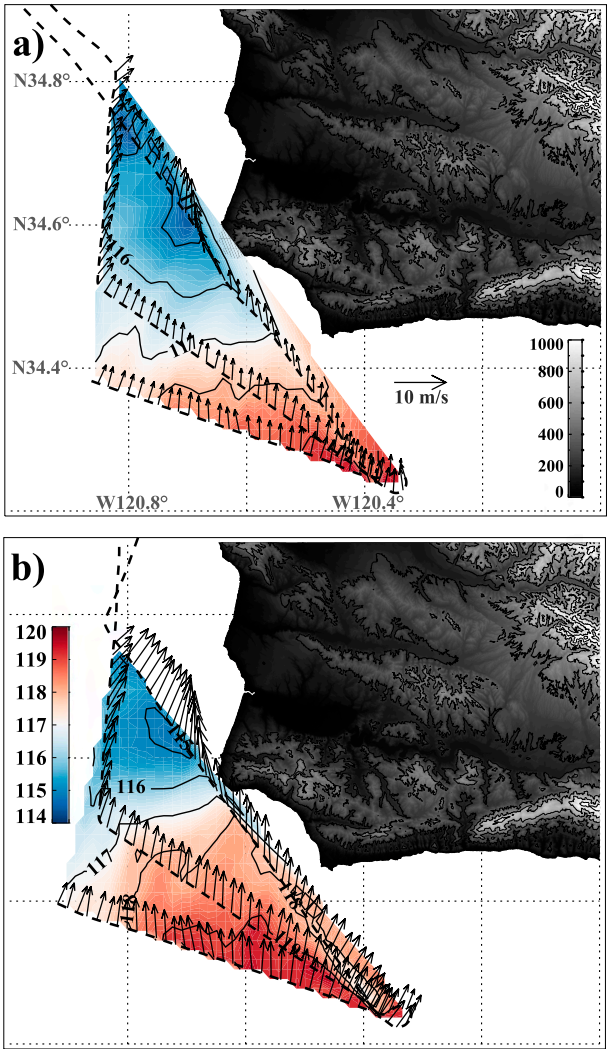

FIG. 6. King Air measurements of 999-hPa heights (color shading, m) from (a) 1809–1902 and (b) 1910–2003 UTC. Flight tracks are shown by the dashed line with wind vectors at 20-s intervals. Topography of California coastal region gray shaded (m).

that decay exponentially offshore to a distance determined by the Rossby radius of deformation. Anomalies of MBL depth correspond to variations in the surface pressure field and these features propagate northward along the coast at a uniform speed. Observations shown here clearly depict this onshore flow that impinges on the coastal mountains north of Point Arguello.

Reasons for the reversal of the alongshore pressure gradient, such as seen for the 16 June 2012 case, are fairly well understood (e.g., Mass and Bond 1996; Ralph et al. 1998; Nuss et al. 2000). A conceptual picture of the large-scale conditions leading to a region of low pressure adjacent to the coast can be found in Ralph et al. (1998). The key is a zone of offshore flow in the atmosphere below about 850 hPa. The role of offshore flow in this case can be investigated with the soundings obtained at the northwest end of the mapping pattern (soundings 6 and 7 and 10 and 11 in Fig. 1). Figure 7a illustrates the temperature, potential temperature, dewpoint, and wind vector profiles from soundings 6 and 7. For comparison, a sounding conducted on 24 May 2012 in nearly the exact location but for strong northerly wind conditions that are typical of the summertime MBL is also shown in Fig. 7a.

For the 16 June case, three distinct layers are present as seen in the potential temperature profile from soundings 6 and 7. The lowest layer we classify as the MBL and it extends from the surface to about 250 m. The MBL is capped by a weak inversion of about 3 K. Winds are directed from the southwest with the strongest winds of about 5 m s^{-1} found in the lower part of the MBL.

The middle layer in soundings 6 and 7 extends from 250 m to about 500 m. Potential temperatures increase by approximately 5°C throughout this layer. Winds are weak and from the south over most of the layer. A strong inversion of about 10 K is present at the top of this middle layer. A sharp contrast in wind occurs across this boundary with winds shifting from a southerly to a northeasterly direction. Wind conditions above about 500 m or so are consistent with offshore flow. The inversion strength is enhanced by the warm air advection and subsidence associated with the offshore flow.

Application of the hypsometric equation shows that a 500-m layer having a temperature 10 K warmer than ambient produces a pressure difference of about 2.0 hPa. From the soundings it is evident that the vertical extent of the warm, offshore flow most likely extends some distance above 1000 m. We conclude that the existence of continental air in the levels above 500 m is sufficient to produce the low pressures north of Point Arguello as seen in Fig. 6.

In contrast, the sounding from the PreAMBLE case of 24 May 2012 also shown in Fig. 7a is representative of the MBL for a strong northerly wind case that is common during the early summer period. In this case, a shallow inversion is observed about 200 m above the ocean that again we view as the top of the MBL. Northwest wind in excess of 20 m s^{-1} is found in this layer with the maximum wind speed at the inversion top. Above the weak inversion, wind speeds decrease rapidly with height. No evidence of offshore flow is present. A major difference is the temperature above the MBL that is roughly 10°C cooler than that seen on 16 June 2012. The temperature difference is a result of the wind direction and source region of the air mass. Winds above the MBL from 24 May sounding are from the north and are of marine origin.

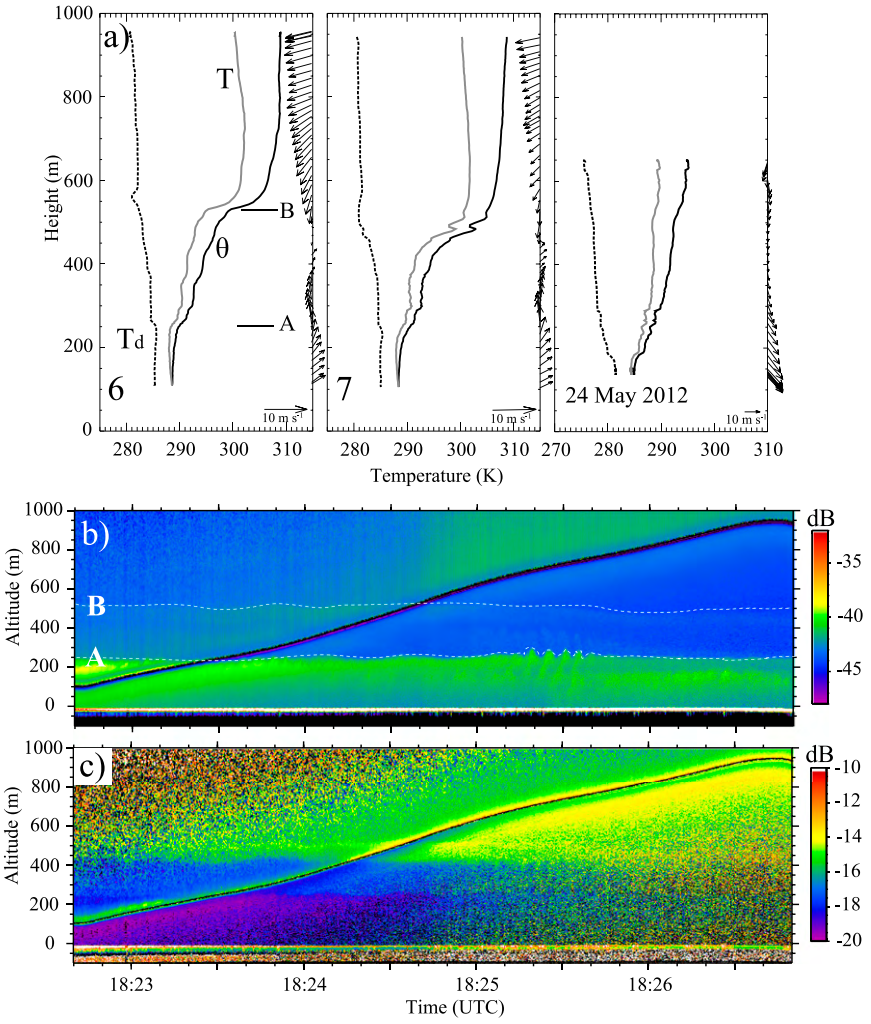

FIG. 7. (a) Soundings 6 and 7 based on King Air measurements during 1823–1831 UTC 16 Jun 2012 located at the northwest end of mapping legs (see Fig. 1 for location) and the sounding at the same location at 1505–1509 UTC 24 May 2012 showing potential temperature (thick, solid line), temperature (thick, gray line), and dewpoint temperature (dashed line) in K, with wind vectors shown on the right side of each sounding. Wyoming Cloud lidar image during 1823–1827 UTC showing (b) copolarized power (dB) and (c) depolarization ratio (dB). Points A and B refer to inversions from soundings and corresponding copolarized lidar returns. The King Air track is indicated by the solid, horizontal line.

Our inferences regarding the boundary layer structure on 16 June 2012 can be confirmed from the WCL copolarized power (Fig. 7b) and depolarization ratio (Fig. 7c). The three-layer structure of the lower atmosphere suggested from the soundings is shown in the subtle, but clearly defined layering in both Figs. 7b and 7c. The depolarization ratio is of particular interest in that variations in aerosol type can be detected and the origin of the air mass can be inferred. High depolarization ratios suggest scattering from irregularly shaped particles such as dust or dry aerosol and are indicative of an air mass of continental origin and lower humidity. Low depolarization ratios usually indicate deliquesced (and therefore spherical) aerosol, likely of marine origin. Strong contrast in the depolarization ratio is observed near the top of the middle layer. The high depolarization values show that the layer above the inversion contains primarily continental aerosol, while the entire layer below the inversion is presumably of marine origin. These inferences are supported by measurements from the PCASP that indicate an increase in aerosol concentration from 190 to over 800 cm^{-3} (not shown) across the inversion. In addition, numerical simulations for this case that are discussed below also support

offshore flow from 600 to 1000 m AGL. Back trajectories from numerical simulations for the sounding locations shown in Fig. 7 indicate flow at 900 hPa having a continental source region.

Soundings were also conducted at the northwest end of leg AB during the second set of mapping legs, roughly 1 hour after soundings shown in Fig. 7. Soundings 10 and 11 (Fig. 8) were taken 1940–1949 UTC, just as the tongue of cloud associated with the southerly surge was advancing northward (Fig. 3a). At the same time skies were clear to the northwest of point B. During the mapping patterns shown in Fig. 6, the upward-pointing lidar detected clouds with bases at about 160 m (about 50 m above flight level) along a 30-km segment of legs AD and AC, matching the satellite imagery shown in Fig. 3a. These clouds later form the leading edge of the southerly surge that propagated past San Francisco by the next morning (Fig. 3). No clouds were observed along line AB during either mapping pattern.

Soundings 10 and 11, shown in Fig. 8, were located north of point B in Fig. 1 and about 30 km north of the advancing cloud boundary. The general features of soundings 10 and 11 are similar to those shown in Fig. 7; again three layers are evident. Close inspection reveals subtle changes during the approximately 80-min interval between soundings $^{6}/_{7}$ and $^{10}/_{11}$. The lower layer of southwest winds has deepened by 50 m or so; likewise, the inversion separating the middle and top layers has increased in height from about 550 to 600 m. Winds show less prominent offshore flow in the layer from 600 to 800 m. The three-layer structure and deepening of the layers are again evident in the lidar copolarized power (Fig. 8b) and depolarization ratio (Fig. 8c). We interpret the deepening of the lower and middle layers as due to the northward progress of the marine layer owing to the horizontal pressure field.

Observations of the vertical structure near the head of the early stages of the southerly surge are similar to the schematic summary of Ralph et al. (2000; cf. their Fig. 13) and confirm the three-layer structure seen in the more mature 10–11 June 1994 event. This is in contrast to a single, deep inversion layer that extends between the lower well-mixed layer and the free troposphere above. Data from the WCL also clearly illustrate these three layers over the entire flight leg and this three-layer structure is likely to extend to a broader area. One of the implications of this difference in structure of the middle layer is the use of the shallow-water equations to represent the system. Typically each layer, whether a two- or three-layer system, is homogeneous and separated by a discontinuity. Ralph et al. (2000) applied a quasi-two-layer system under two different assumptions to account for the three layers that included the MBL, a middle layer containing the deep inversion layer, and the free troposphere.

4. Simulation of the initiation of the 16–17 June 2012 wind reversal

a. *Overview*

Numerical simulation of the 16–17 June 2012 surge was conducted using WRF version 3.5.1 (e.g., Skamarock et al. 2008). Three domains were used that were centered over the California coast just south of Monterey Bay. Horizontal grid resolutions of 18, 6, and 2 km were employed; the innermost domain consists of 289 × 319 grid points covering an area that contains the surge from its inception until it ceases northward progression approximately 100 km north of San Francisco. A vertical grid of 84 sigma levels was used with increasing resolution toward the surface.

As with previous modeling studies of the MBL associated with a coastally trapped wind reversal (e.g., Rahn and Parish 2008; Rahn and Parish 2010), choice of planetary boundary layer and cloud parameterizations critically influence the wind and temperature fields. This, in turn, impacts significantly the development of stratus clouds and propagation of surge along the coast. Extensive sensitivity testing was also conducted concerning the low stratus clouds observed during episodes of the Catalina eddy circulation (e.g., Parish et al. 2013). Key parameterizations used for the run are the following: the Lin (Purdue) microphysics scheme, the new Goddard scheme for longwave and shortwave radiation physics, the MM5 surface layer similarity with the unified Noah land surface model, and the Yonsei University boundary layer physics scheme.

We would like to stress that this particular configuration produced results that most closely fit our observations, but does not mean that this set of parameterizations will consistently produce the best results on other days and under different forcing. In some cases, the model can fail to produce output that agrees with observations [cf. Fig. 15 in Rahn et al. (2014)]. Measurements obtained during PreAMBLE provide a very challenging test for numerical simulations. Given the rich diversity of mesoscale processes that can impact the lower atmosphere in this region, understanding the root cause of the model deficiencies is not a trivial undertaking, but one worth pursuing.

For this case, the model was initialized at 0000 UTC 16 June 2012 using the 0.5° horizontal resolution Global Forecast System grids. Lateral boundary conditions were specified at 6-h intervals and the simulation was run for 42 h. For brevity, only details from the 2-km domain are presented for times coincident with the aircraft observations and those associated with the surge initiation.

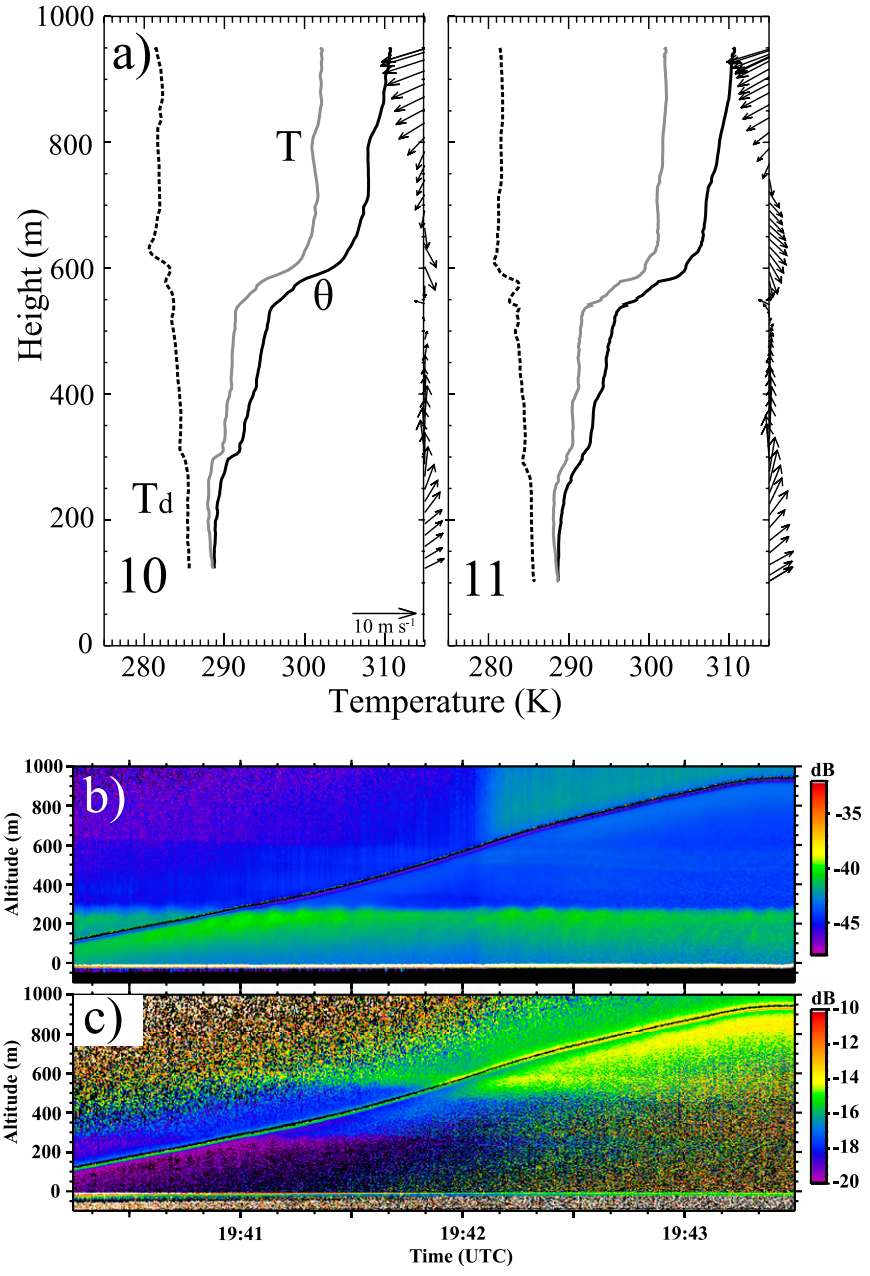

FIG. 8. (a) Soundings 10 and 11 based on King Air measurements during 1940–1949 UTC 16 Jun 2012 located at the northwest end of mapping legs (see Fig. 1 for location) showing potential temperature (thick, solid line), temperature (thick, gray line), and dewpoint temperature (dashed line) in K, with wind vectors shown on the right side of each sounding. Wyoming Cloud lidar image during 1940–1944 UTC showing (b) copolarized power (dB) and (c) depolarization ratio (dB). The King Air track is indicated by the solid, horizontal line.

Progression of the low stratus is one of the more difficult aspects to simulate. Figure 9 presents an overview of the results, showing the WRF-simulated low-level stratus associated with the southerly surge at 3-h increments during the early morning hours of 17 June 2012 as compared with GOES-West satellite imagery from the Naval Research Laboratory. Northward progression of the coastal stratus was most apparent during this 9-h period. WRF is able to simulate the extent and propagation speed of the surge with fidelity. The pouring of the stratus clouds into Monterey Bay at 0900 UTC (Fig. 9d) is especially well simulated. Given that WRF is

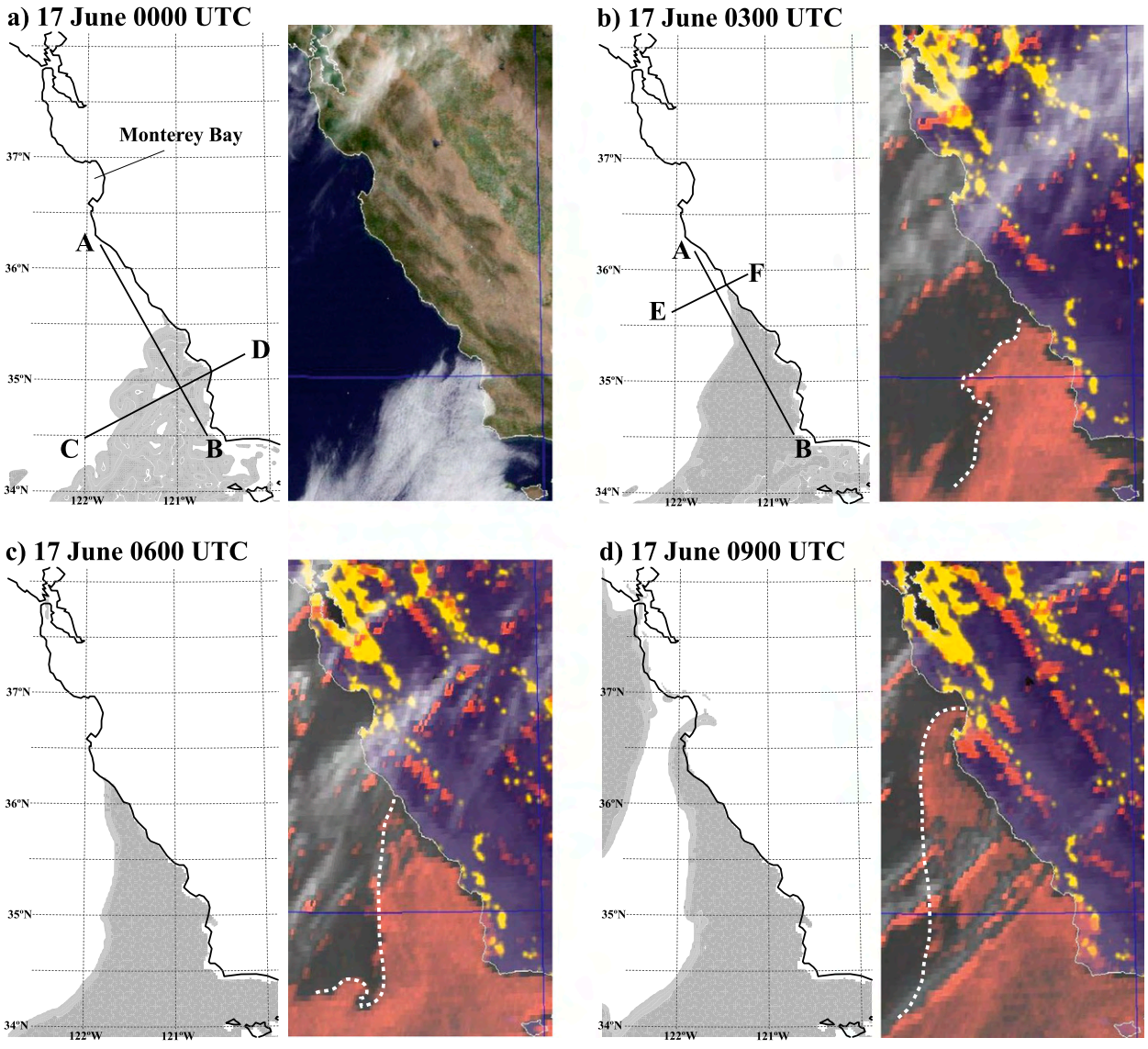

FIG. 9. Comparison of (left) WRF-simulated stratus with (right) GOES-West satellite image from Naval Research Laboratory at (a) 0000, (b) 0300, (c) 0600, and (d) 0900 UTC 17 Jun 2012. The estimated surge boundary in satellite imagery is indicated by the dashed white line. The solid black lines indicate the location of cross sections to be described later.

able to capture the essential features of the surge, an assumption is that the key governing physics of the wind reversal are also well replicated.

b. Comparison with aircraft observations

The fundamental observational feature of the pre-surge environment is the reversal of the horizontal pressure field from that normally seen during summer. Higher pressure situated to the south of Point Arguello and lower pressure to the north is the impetus for the initiation of the low-level stratus surge. Direct comparison of WRF output with King Air observations can be made by examination of the 999-hPa height and wind fields at 1900 and 2000 UTC (Fig. 10), representative of the times during which the height field was being mapped by the King Air. At 1900 UTC (Fig. 10a), the reversal in the height field is seen in WRF results, similar to that from the King Air analyses in Fig. 6 except that the gradient is a bit less pronounced in the model simulation. The 999-hPa height gradient does increase by 2000 UTC (Fig. 10b) similar to that observed. The focus of the height contours and the strong height gradient near Point Arguello is well resolved.

Winds at the 999-hPa level in the WRF simulation are in accord with King Air observations and match the Skamarock et al. (1999, cf. their Fig. 17) conceptual

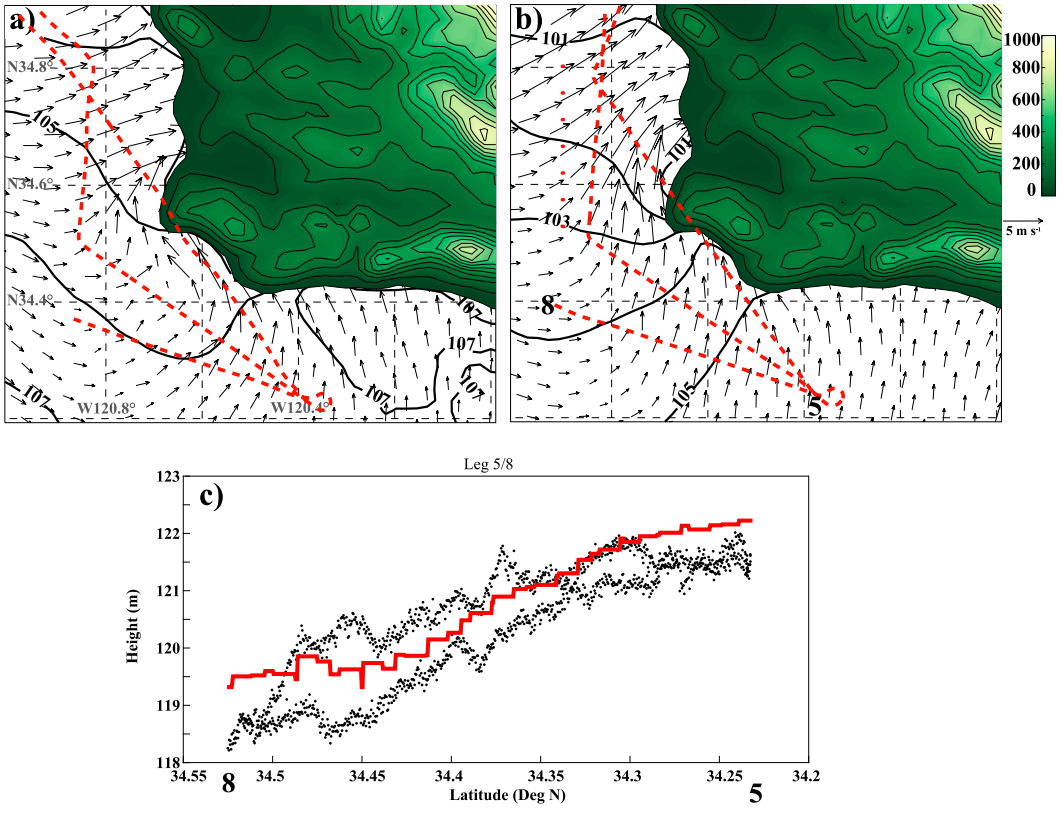

FIG. 10. WRF-simulated 999-hPa heights (dark, solid lines; m) and wind vectors from innermost domain at (a) 1900 and (b) 2000 UTC 16 Jun 2012, corresponding to times from King Air analysis shown in Fig. 6. WRF terrain heights (m) are shown by the color shading. The King Air flight track is shown by the red, dashed line. (c) Comparison of WRF 999-hPa height (m) from legs 5 and 8 (black dots) and the 2000 UTC model height (offset +6 m) along the leg (red line).

picture of the initiation of a surge. Strongest winds are found north of Point Arguello with winds directed increasingly toward the coast. Acceleration of the flow from south to north such as seen in the King Air data is also well resolved. Wind speeds from the King Air observations as well as in WRF are in the 4–8 m s^{-1} range with the simulated winds being somewhat weaker than those observed. Wind directions from the WRF output are consistent with the King Air data. Impingement of the 999-hPa flow against the coastal mountains north of Point Arguello is clearly shown. The WRF-simulated height change along legs 5 and 8 matches well with the King Air observations (Fig. 10c). The subsequent blocking of the flow by the coastal mountains in WRF helps initiate the northward propagation of the surge similar to that discussed by Ralph et al. (1998) and Skamarock et al. (1999).

c. *Cross-coast atmospheric structure during the initiation phase*

Key features in the King Air observations as well as the WRF simulation are the northward-directed pressure gradient force and the resulting ageostrophic motion. Observations and results from the WRF simulation indicate that low-level winds to the north of Point Arguello are directed nearly orthogonal to the coastal mountains. As this stable air reaches the coastal mountains, blocking must occur with a subsequent flow deflection northward that becomes the southerly surge.

To better depict the dynamics of the surge initiation, an emphasis is placed on the pressure field associated with the WRF simulation. The following analyses depict perturbations of the isobaric height field as a means to display the vertical structure of the horizontal pressure gradient force. Such isobaric height perturbations are similar to D values (Bellamy 1945), which are departures of an isobaric height from the respective mean isobaric height of the *U.S. Standard Atmosphere, 1976* (COESA 1976). Here isobaric height perturbations are computed by first determining the mean isobaric height at each level at the 1600 UTC 16 June 2012 time and then subtracting those mean values from actual heights at the respective isobaric levels for each time period. Choice of the 1600 UTC 16 June time to compute averages was made as representative of the atmosphere just prior to the surge. All isobaric height perturbations provide a measure of relative changes from the presurge

environment. The essential feature of the analyses is that variations of height along an isobaric surface are proportional to horizontal variations of pressure along a constant height surface; each is a measure of the horizontal pressure gradient force. Use of isobaric perturbation heights allows inspection of the horizontal pressure gradient force at all levels when examining cross sections.

To explore the initiation phase of the surge, cross sections normal to the terrain have been prepared based on the WRF simulations. Figure 11 presents a series of cross sections situated just west of the surge stratus and crossing south of Point Buchon (line CD in Fig. 9) at times just prior to the northward propagation of the surge. Cross-coast wind components, isobaric height perturbations, and potential temperatures are illustrated in the cross section. At 2000 UTC (Fig. 11a), corresponding to the time of the second King Air mapping mission, wind components directed onshore are prevalent in the lowest 200 m over the entire cross section. The depth of onshore winds increases toward the coast. Maximum cross-coast wind components greater than $4\,m\,s^{-1}$ are found in the lowest 200 m within 20 km or so of the coastal mountains. Offshore flow is present above about 500 m, consistent with the King Air soundings such as that shown in Fig. 8.

Cross-coast winds directed toward the coastline are in response to the pressure field. Inspection of Fig. 11a shows lowest isobaric height perturbations tucked in against the coastal mountains at a height of about 500 m. The cross-coast horizontal pressure gradient force throughout the cross section is directed toward the east; strongest gradients are seen in the lowest 500 m. Isobaric perturbation heights at 2000 UTC 16 June (Fig. 11a) show little evidence of blocking. There is only a suggestion in the potential temperature field of some blocking right at the coast as isentropes become deflected upward.

By 2200 UTC (Fig. 11b), the maximum cross-coast wind components have reached the coast. Blocking of the stable marine air by the coastal terrain is apparent. Isobaric height perturbations adjacent to the coast have increased and the onshore horizontal pressure gradient force in the lower atmosphere has decreased; height perturbations within about 50 km of the coast have increased by several meters and the isobaric slopes have been reduced to near zero. Development of an alongshore component of the flow (not shown) first appears adjacent to the coastal mountains at about 300 m, coincident with the cross-coast wind maxima and in response to the flows impinging on the barrier. Potential temperatures also begin to show increasing evidence of terrain blocking, clearly displaced upward near the coast.

During the next 4 hours, blocking becomes more apparent. By 0200 UTC 17 June (Fig. 11d), corresponding to the approximate time that the southerly surge started its northward propagation, a pronounced blocking is present as evidenced by the upward sloping to the east of the isobaric height perturbations within about 50 km of the coast. In response to an increasingly adverse horizontal pressure gradient force, the onshore components of the wind decrease in intensity and areal extent by 0200 UTC 17 June. Weak alongshore components (not shown) begin to develop by 0000 UTC 17 June and are approximately $2\,m\,s^{-1}$ in the lower 200 m within a roughly 50-km-wide zone adjacent to the coast by 0200 UTC. The pronounced adjustment of the isobaric perturbation height field in response to the impingement of cross-coast flows against the coastal mountains marks the commencement of the surge.

d. *Alongshore atmospheric structure during the initiation phase*

To illustrate the structure of the lower atmosphere in an alongshore direction, cross sections at 2000 and 2200 UTC 16 June and 0000 and 0300 UTC 17 June have been prepared (see line AB in Fig. 9). Cross-coast and alongshore wind components during the initiation phase are shown in Fig. 12. The southern point in the cross section is situated just west of Point Arguello. The turning of the flow from southeast to west around Point Arguello (e.g., Fig. 10) is apparent in the lowest few hundred meters at the southern edge of the cross section at 2000 UTC (Fig. 12a). Onshore flow is present over most of the lower atmosphere with the maximum found just north of Point Arguello. Offshore flow at 2000 UTC 16 June is maximized above 700 m at a distance of about 50 km on the scale shown in Fig. 12a, corresponding to a point southwest of Point Buchon and near the intersection of the cross section CD in Fig. 9. Southerly flow first develops several hundred meters above the ocean and is strongest as it turns north around Point Arguello, but becomes increasingly disorganized at low levels to the north. North winds are strongest near the surface and extend from the most northern point in the cross section to Point Buchon near the 70-km distance on the scale shown in Fig. 12.

Northward progress of both cross-coast and alongshore wind components can be seen in subsequent time periods. Onshore winds remain present in the lower atmosphere throughout the period. Offshore winds decrease considerably by 2200 UTC 16 June (Fig. 12b) and disappear in the lowest 700 m by 0000 UTC 17 June (Fig. 12c). Northward-directed alongshore components at low levels remain disorganized until about 0300 UTC 17 June (Fig. 12d).

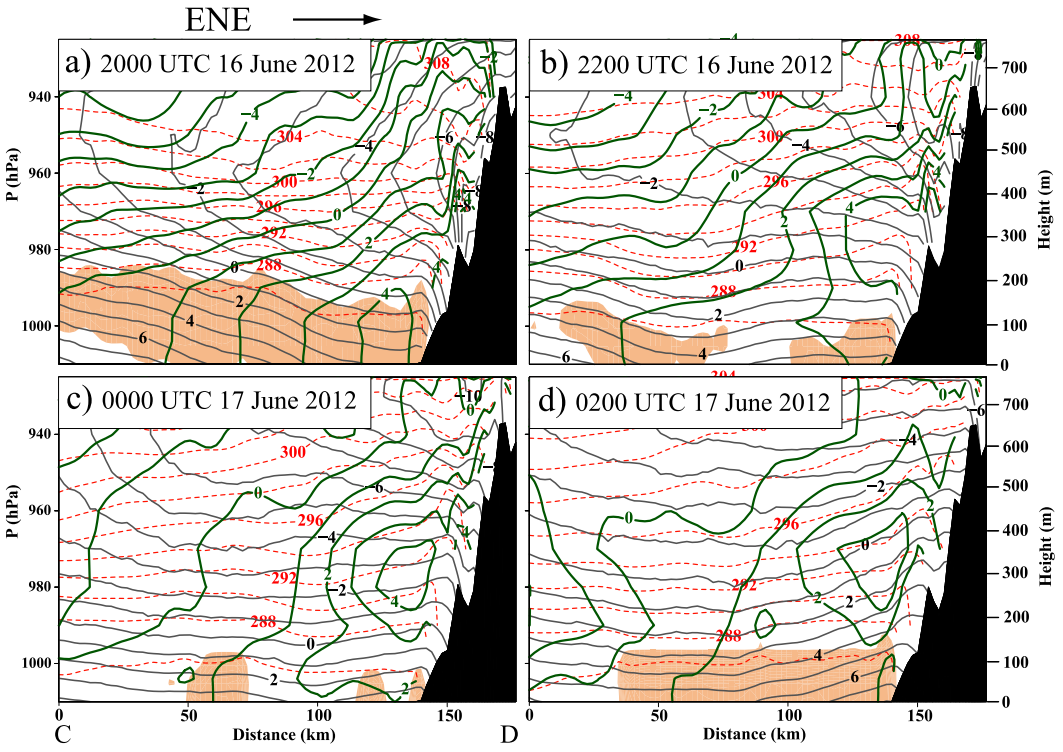

FIG. 11. WRF-simulated isobaric height perturbations (black solid lines, m), potential temperatures (red dashed lines, K), and cross-coast wind components (green solid lines, m s^{-1}, positive values toward coast) for cross section normal to the coast shown by line CD in Fig. 9 (distances directed toward ENE from C to D) for (a) 2000 and (b) 2200 UTC 16 Jun, and (c) 0000 and (d) 0200 UTC 17 Jun 2012. The coastal mountains are indicated by the dark shading; the stratus layer is indicated by the tan shading.

To depict the northward forcing of the surge, alongshore cross sections of potential temperature and isobaric height perturbation fields have also been prepared along the same line (AB in Fig. 9). Isobaric height perturbations reveal several key features. At 2000 UTC (Fig. 13a) a local minimum in isobaric height perturbations is present at a height of 200 m above the ocean north of Point Arguello. Such a minimum corresponds to the highest potential temperatures at that level and is the result of offshore advection of warm air. Analyses (not shown) reveal that warming in WRF in the marine environment just offshore from the coast is dominated by warm air advection, a finding similar to that discussed by Ralph et al. (1998) and Rahn and Parish (2008).

Note that the isobaric height perturbation minimum is tilted upward toward the south throughout the initiation of the surge. Soundings conducted by the King Air (e.g., Fig. 7a, sounding locations correspond to distances of 30–40 km for the scale shown in Fig. 13) are consistent with this analysis; offshore flow and warm air advection are found at heights above about 500 m.

A primary south–north gradient in the isobaric height perturbations is apparent in the lowest couple hundred meters or so ahead of the surge for all times shown. We view this gradient as the key driver of the surge. This northward forcing is strongest within the lowest 200 m or so and decreases with height. The steepest slopes of the isobaric height perturbation surfaces, indicative of the strongest horizontal pressure gradient forces, are seen ahead of the actual surge stratus. Isobaric height perturbations increase in general to the south with the largest increases in the lower atmosphere. The horizontal pressure gradient force switches sign above about 500 m and is directed such that higher heights are to the north.

The surge advances and by 0300 UTC 17 June (Fig. 13d) the stratus lags the actual wind reversal in the WRF simulations by about 50 km, consistent with the results in Thompson et al. (2005). They show that at the leading edge of the southerly surge there is a zone of convergence between the wind shift and the cloud/fog to the south. This convergence zone is what preconditions the environment by lifting the shallow mixed layer and increasing the relative humidity toward the south until producing the cloud/fog. This zone explains the lag between the arrival of the wind shift and cloud/fog layer. The isobaric height perturbation minimum

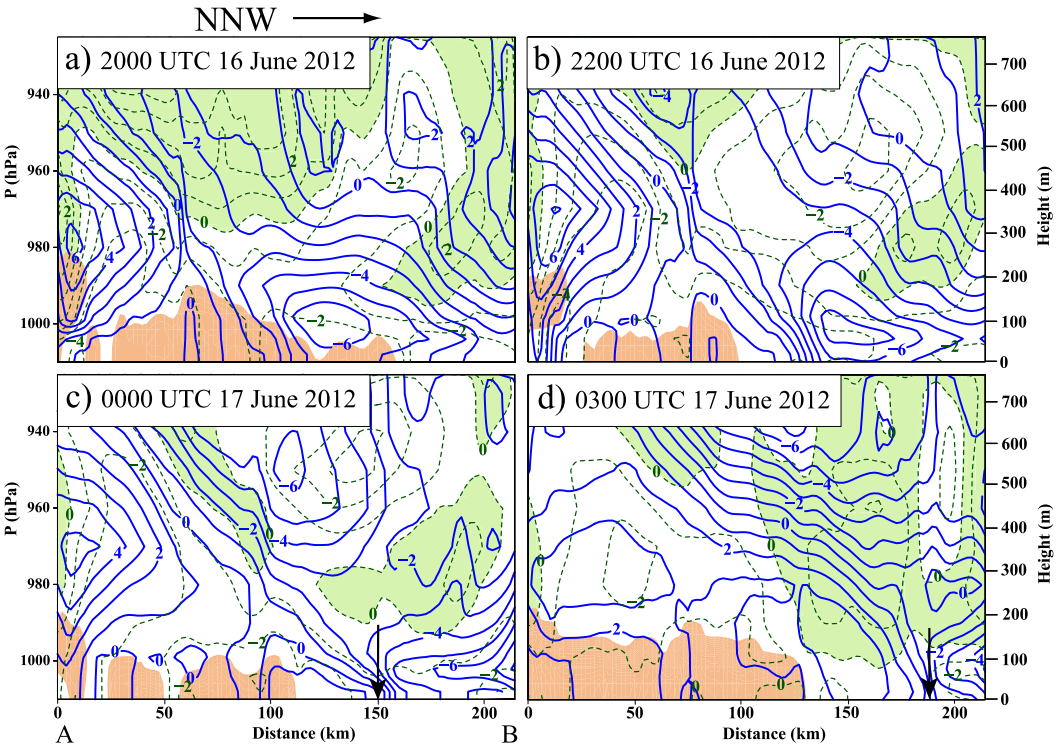

FIG. 12. WRF-simulated alongshore wind components (blue solid, m s^{-1}, positive values toward the north) and cross-coast wind components (green dashed lines, m s^{-1}, positive values away from the coast) for alongshore cross section shown by line AB on Fig. 9 (distances directed toward NNW from A to B) for (a) 2000 and (b) 2200 UTC 16 Jun, and (c) 0000 and (d) 0300 UTC 17 Jun 2012. The dark arrows indicate the head of wind reversal. The offshore flow is indicated by the light green shading; the stratus layer is indicated by the tan shading.

displays a northward progression, consistent with the northward propagation of the surge. From Fig. 13, the minimum isobaric height perturbation moves approximately 5 m s^{-1} from 2000 to 2200 UTC 16 June and somewhat faster during subsequent nighttime hours. This northward progression of the pressure field in surge events has been noted by others (e.g., Ralph et al. 1998).

Potential temperatures shown in Fig. 13 reveal a dramatic contrast in the alongshore boundary layer structure, especially just prior to the surge initiation. Little evidence of a well-mixed MBL is seen ahead of the reversal at the initiation stage of the surge at 2000 UTC 16 June (Fig. 13a). With offshore flow, the MBL has nearly collapsed. In this sense, the description in Nuss et al. (2000) of "a cool marine layer to the south along the coast with little or no marine layer to the north" is appropriate. As the surge begins to move northward (Fig. 13d), it retains characteristics of a well-mixed boundary layer capped by an inversion.

e. Cross-coast structure near the head of the surge

Results from the WRF simulation provide a realistic portrayal of the northward progression of the surge. The response of the atmosphere near the head of the surge in the 6-h period preceding the event is examined using a cross section normal to the coast (line EF in Fig. 9) and is shown in Fig. 14. At 2200 UTC 16 June 2012 (Fig. 14a), alongshore winds from the north exist throughout the lower atmosphere with a maximum speed of about 7 m s^{-1} between 100 and 200 m above the ocean. Isobaric height perturbations show a minimum adjacent to the coast in the lower levels of the atmosphere. The cross-coast component of the horizontal pressure gradient force is thus directed toward the coast below 300 m. Isentropic surfaces slope slightly downward to the coast.

By 0000 UTC 17 June 2012 (Fig. 14b), few changes are apparent in the isobaric height perturbation field in WRF with the horizontal pressure gradient force still directed onshore. Isentrope orientation remains horizontal in the cross-coast direction. Winds remain northerly in the lower atmosphere.

First evidence of the surge can be seen in the WRF alongshore wind components at 0200 UTC 17 June (Fig. 14c) in which weak southerly flow appears adjacent to the coast in the lowest 100 m or so. Note that the isobaric height perturbations in the lowest 200 m no

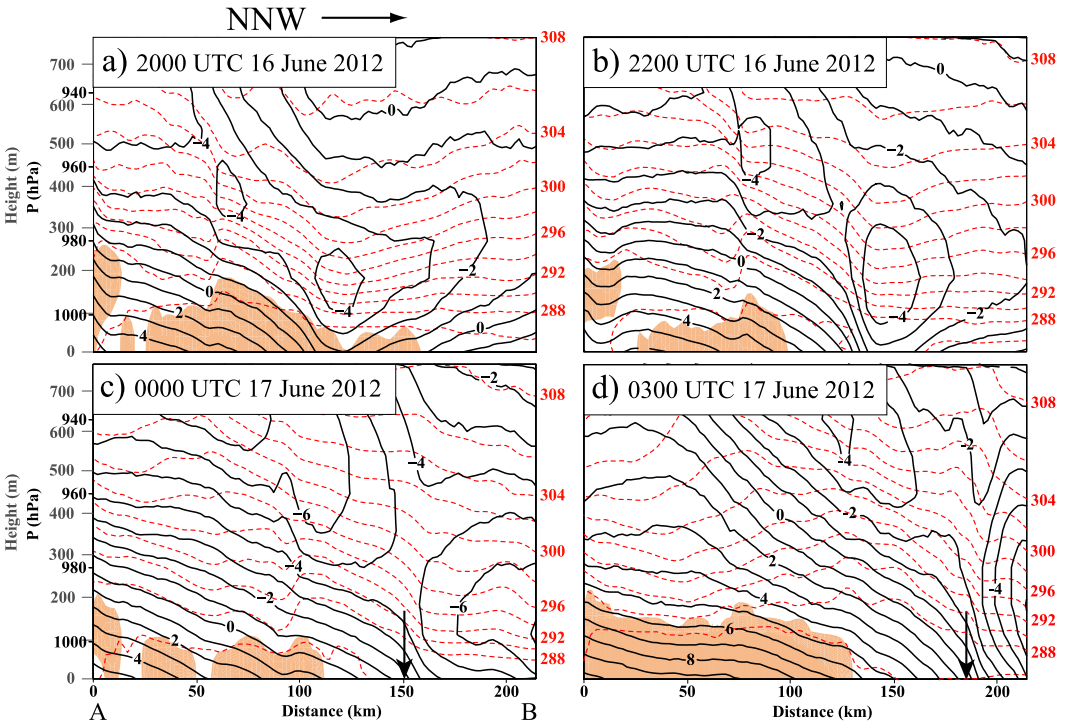

FIG. 13. WRF-simulated isobaric height perturbations (black solid lines, m) and potential temperatures (red dashed lines, K) for alongshore cross section shown by line AB on Fig. 9 (distances directed toward NNW from A to B) for (a) 2000 and (b) 2200 UTC 16 Jun, and (c) 0000 and (d) 0300 UTC 17 Jun 2012. The dark arrows indicate the head of wind reversal; the stratus layer is indicated by the tan shading.

longer show a horizontal pressure gradient directed toward the coast, being directed nearly horizontal. Actual perturbation height values are increasing at the surface. By 0400 UTC (Fig. 14d) the head of the surge stratus has reached line EF. The surge wind field is now well organized with a maximum alongshore speed of nearly $8\,m\,s^{-1}$ positioned adjacent to the coastal terrain. The zone of northward-directed flows has expanded to roughly 60 km in width. Surface pressures continue to rise as evidenced by increasing values of the isobaric perturbation heights. We view this phase of the flow as antitriptic in nature, being accelerated in response to the alongshore horizontal pressure gradient force in the lowest layers of the atmosphere such as illustrated in Fig. 13d. Note that isentropic surfaces in the lowest 300 m show a significant rise during the previous two hours. This is consistent with the general isentropic slopes that increase toward the south in the alongshore cross section (Fig. 13) that suggest a deeper marine layer to the south.

5. Summary

The southerly surge of 16–17 June 2012 progressed along the California coast from Point Arguello to the north of San Francisco over a roughly 12-h period. As with other southerly surges, most of the movement of the low stratus occurred during the nighttime hours. The tendency for surging overnight into the morning was observed in the climatology of Bond et al. (1996). Greater forcing overnight is thought to be due in part to differences in the radiation budget between the clear skies ahead of the surge and the fog/low cloud of the surge. During the night the cloud-top radiational cooling deepens and cools the boundary layer within the surge, thus increasing the alongshore pressure gradient and increasing the propagation speed (Rahn and Parish 2008). The surge was not well forecast from operational models. One of the authors (DAR), convinced that initiation of a southerly surge was imminent, ordered a King Air research flight.

Analysis of aircraft data shows that the horizontal pressure gradient force in the Santa Barbara Channel becomes reversed from the climatological mean. For the 16 June 2012 case, pressures increase toward the east. As a result, winds in the channel are directed primarily from the east. The focus area for the flight was the marine environment at the western end of the Santa Barbara Channel and extending northward. Results from the airborne mapping legs showed a horizontal pressure

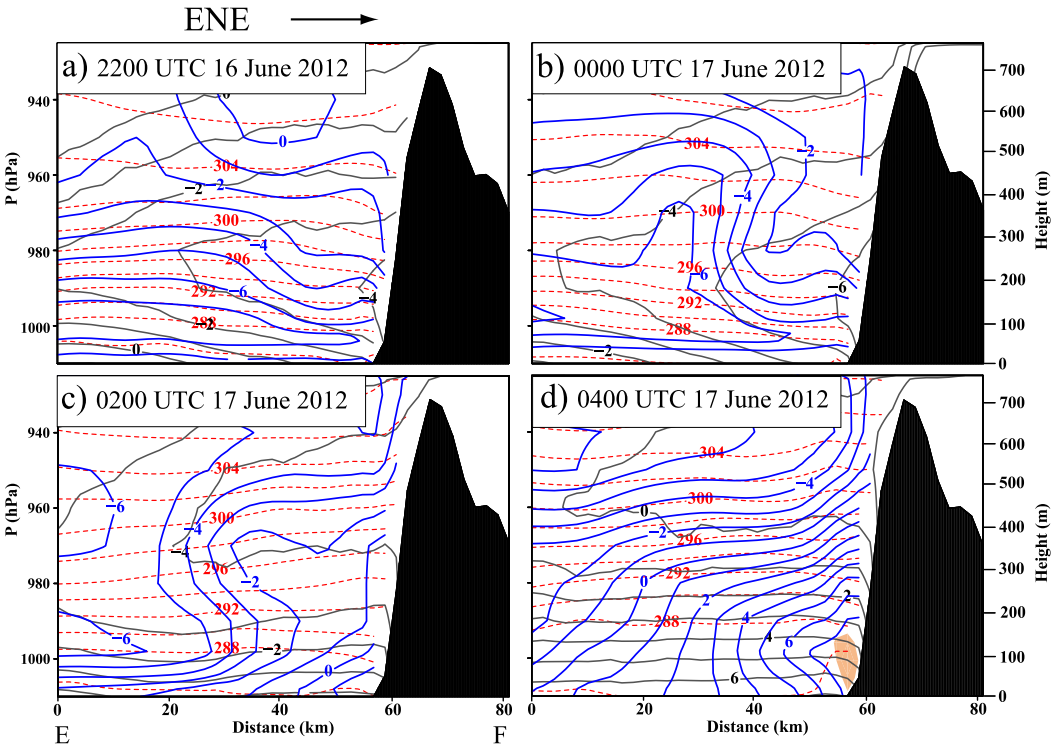

FIG. 14. WRF-simulated isobaric height perturbations (black solid lines, m), potential temperature (red dashed lines, K), and alongshore wind components (blue solid lines, m s^{-1}, positive values for south wind) for cross section normal to coast shown by line EF in Fig. 9 for (a) 2200 UTC 16 Jun and (b) 0000, (c) 0200, and (d) 0400 UTC 17 Jun 2012. The coastal mountains are indicated by the dark shading; the stratus layer is indicated by the tan shading.

gradient that was directed northward with a minimum in pressure just west of the coast north of Point Arguello. This pressure gradient force supports a northward acceleration of the flow. Such a pressure field has been suggested for some time although this is the first time airborne mapping has been conducted associated with a surge.

Development of the horizontal pressure field is linked to advection of warm, dry continental air over the marine environment. Effects of such preconditioning are seen in aircraft soundings that show northeasterly winds and temperatures show that the zone of low pressure adjacent to the coast results from the advection of warm, continental air in a layer above about 600 m. The inferred isobaric height field is consistent with satellite-observed motion of the stratus field and the surface pressure from buoy and surface stations along the coast (not shown).

The south–north pressure gradient force is in contrast with the climatological norm. The pressure field supports the motion of low-level marine air that represents the initial stage of the southerly surge. Winds measured during the mapping mission are highly ageostrophic, being directed in a downgradient manner. The marine flow accelerates to the north and east, directed with a significant component normal to the coastline and hence coastal mountains. Satellite imagery shows that as the cool, cloudy marine air impinges against the coastal terrain north of Point Arguello, it becomes blocked by the mountains and heads north along the coast to start the surge. Northward propagation of stratus along the coast became apparent in the satellite imagery by 0000 UTC 17 June although the northward movement of clouds south of Point Arguello is present in satellite imagery toward the end of the research flight at 2030 UTC 16 June.

WRF simulations of the wind and isobaric height fields are in reasonable agreement with the King Air observations. Numerical results show that the blocking by the coastal terrain north of Point Arguello produce a pressure surplus that supports a northward acceleration of the flow. The southerly surge moves in response to a northward-directed horizontal pressure gradient force. The flow can be characterized as a downgradient, ageostrophic motion similar to antitriptic motion. Such a surge is dependent on a supportive horizontal pressure field as it propagates northward. This speaks to the importance of the large-scale flow in establishing a

favorable low-level environment that permits northward movement of air in the coastal region.

Acknowledgments. This research was supported in part by the National Science Foundation through Grants AGS-1034862, AGS-1439515, and AGS-1439594. The authors wish to thank pilots Ahmad Bandini and Brett Wadsworth and scientists Jeff French and Larry Oolman for help with the PreAMBLE field study and King Air measurements.

REFERENCES

Bane, J. M., 1997: Airflow and stratification in propagating southerly surges within the summertime marine layer off California and Oregon. Preprints, *12th Symp. on Boundary Layers and Turbulence*, Vancouver, BC, Canada, Amer. Meteor. Soc., 346–347.

Beardsley, R. C., C. E. Dorman, C. A. Friehe, L. K. Rosenfeld, and C. D. Winant, 1987: Local atmospheric forcing during the Coastal Ocean Dynamics Experiment 1. A description of the marine boundary layer and atmospheric conditions over a northern California upwelling region. *J. Geophys. Res.*, **92**, 1467–1488, doi:10.1029/JC092iC02p01467.

Bellamy, J. C., 1945: The use of pressure altitude and altimeter corrections in meteorology. *J. Meteor.*, **2**, 1–79, doi:10.1175/1520-0469(1945)002<0001:TUOPAA>2.0.CO;2.

Bond, N. A., C. A. Mass, and J. E. Overland, 1996: Coastally trapped wind reversals along the United States West Coast during the warm season. Part I: Climatology and temporal evolution. *Mon. Wea. Rev.*, **124**, 430–445, doi:10.1175/1520-0493(1996)124<0430:CTWRAT>2.0.CO;2.

Burk, S. D., and W. T. Thompson, 1996: The summertime low-level jet and marine boundary layer structure along the California coast. *Mon. Wea. Rev.*, **124**, 668–686, doi:10.1175/1520-0493(1996)124<0668:TSLLJA>2.0.CO;2.

Cai, Y., J. R. Snider, and P. Wechsler, 2013: Calibration of the passive cavity aerosol spectrometer probe for airborne determination of the size distribution. *Atmos. Meas. Tech. Discuss*, **6**, 4123–4152, doi:10.5194/amtd-6-4123-2013.

COESA, 1976: *U.S. Standard Atmosphere, 1976*. NOAA, 227 pp.

Dorman, C. E., 1985: Evidence of Kelvin waves in California's marine layer and related eddy generation. *Mon. Wea. Rev.*, **113**, 827–839, doi:10.1175/1520-0493(1985)113<0827:EOKWIC>2.0.CO;2.

——, and D. Koračin, 2008: Response of the summer marine layer flow to an extreme California coastal bend. *Mon. Wea. Rev.*, **136**, 2894–2922, doi:10.1175/2007MWR2336.1.

Hsu, H.-M., L.-Y. Oey, W. Johnson, C. Dorman, and R. Hodur, 2007: Model wind over the central and southern California coastal ocean. *Mon. Wea. Rev.*, **135**, 1931–1944, doi:10.1175/MWR3389.1.

Koračin, D., and C. E. Dorman, 2001: Marine atmospheric boundary divergence and clouds along California in June 1996. *Mon. Wea. Rev.*, **129**, 2040–2056, doi:10.1175/1520-0493(2001)129<2040:MABLDA>2.0.CO;2.

Lenschow, D. H., E. R. Miller, and R. B. Friesen, 1991: A three-aircraft comparison of two types of air motion measurement systems. *J. Atmos. Oceanic Technol.*, **8**, 41–50, doi:10.1175/1520-0426(1991)008<0041:ATAIOT>2.0.CO;2.

Mass, C. F., and M. D. Albright, 1987: Coastal southerlies and alongshore surges of the west coast of North America: Evidence of mesoscale topographically trapped response to synoptic forcing. *Mon. Wea. Rev.*, **115**, 1707–1738, doi:10.1175/1520-0493(1987)115<1707:CSAASO>2.0.CO;2.

——, and N. Bond, 1996: Coastally trapped wind reversals along the west coast during the warm season. Part II: Synoptic evolution. *Mon. Wea. Rev.*, **124**, 446–461, doi:10.1175/1520-0493(1996)124<0446:CTWRAT>2.0.CO;2.

——, and W. J. Steenburgh, 2000: An observational and numerical study of an orographically trapped wind reversal along the West Coast of the United States. *Mon. Wea. Rev.*, **128**, 2363–2397, doi:10.1175/1520-0493(2000)128<2363:AOANSO>2.0.CO;2.

Nuss, W. A., 2007: Synoptic-scale structure and the character of coastally trapped wind reversals. *Mon. Wea. Rev.*, **135**, 60–81, doi:10.1175/MWR3267.1.

——, and Coauthors, 2000: Coastally trapped wind reversals: Progress toward understanding. *Bull. Amer. Meteor. Soc.*, **81**, 719–743, doi:10.1175/1520-0477(2000)081<0719:CTWRPT>2.3.CO;2.

Parish, T. R., 2000: Forcing of the summertime low-level jet along the California coast. *J. Appl. Meteor.*, **39**, 2421–2433, doi:10.1175/1520-0450(2000)039<2421:FOTSLL>2.0.CO;2.

——, and D. Leon, 2013: Measurement of cloud perturbation pressures using an instrumented aircraft. *J. Atmos. Oceanic Technol.*, **30**, 215–229, doi:10.1175/JTECH-D-12-00011.1.

——, M. D. Burkhart, and A. R. Rodi, 2007: Determination of the horizontal pressure gradient force using global positioning system onboard an instrumented aircraft. *J. Atmos. Oceanic Technol.*, **24**, 521–528, doi:10.1175/JTECH1986.1.

——, D. A. Rahn, and D. Leon, 2008: Aircraft observations of a coastally trapped wind reversal off the California coast. *Mon. Wea. Rev.*, **136**, 644–662, doi:10.1175/2007MWR2199.1.

——, ——, and ——, 2013: Airborne observations of a Catalina eddy. *Mon. Wea. Rev.*, **141**, 3300–3313, doi:10.1175/MWR-D-13-00029.1.

——, ——, and ——, 2014: Airborne observations of the marine boundary layer adjustment near Point Arguello, California. *J. Appl. Meteor. Climatol.*, **53**, 970–989, doi:10.1175/JAMC-D-13-0164.1.

Pomeroy, K. R., and T. R. Parish, 2001: A case study of the interaction of the summertime coastal jet with the California topography. *Mon. Wea. Rev.*, **129**, 530–539, doi:10.1175/1520-0493(2001)129<0530:ACSOTI>2.0.CO;2.

Rahn, D. A., and T. R. Parish, 2007: Diagnosis of the forcing and structure of the coastal jet near Cape Mendocino using in situ observations and numerical simulations. *J. Appl. Meteor. Climatol.*, **46**, 1455–1468, doi:10.1175/JAM2546.1.

——, and ——, 2008: A study of the forcing of the 22–25 June 2006 coastally trapped wind reversal based on numerical simulations and aircraft observations. *Mon. Wea. Rev.*, **136**, 4687–4708, doi:10.1175/2008MWR2361.1.

——, and ——, 2010: Cessation of the 22–25 June 2006 coastally trapped wind reversal. *J. Appl. Meteor. Climatol.*, **49**, 1412–1428, doi:10.1175/2010JAMC2242.1.

——, ——, and D. Leon, 2014: Coastal jet adjustment near Point Conception, California, with opposing wind in the bight. *Mon. Wea. Rev.*, **142**, 1344–1360, doi:10.1175/MWR-D-13-00177.1.

Ralph, F. M., L. Armi, J. M. Bane, C. E. Dorman, W. D. Neff, P. J. Neiman, W. A. Nuss, and P. O. G. Persson, 1998: Observations and analysis of the 10–11 June 1994 coastally trapped disturbance. *Mon. Wea. Rev.*, **126**, 2435–2465, doi:10.1175/1520-0493(1998)126<2435:OAAOTJ>2.0.CO;2.

——, P. J. Neiman, J. M. Wilczak, P. O. G. Persson, J. M. Bane, M. L. Cancillo, and W. Nuss, 2000: Kelvin waves and internal

bores in the marine boundary layer inversion and their relationship to coastally trapped wind reversals. *Mon. Wea. Rev.*, **128**, 283–300, doi:10.1175/1520-0493(2000)128<0283:KWAIBI>2.0.CO;2.

Rogers, D. P., and Coauthors, 1998: Highlights of Coastal Waves 1996. *Bull. Amer. Meteor. Soc.*, **79**, 1307–1326, doi:10.1175/1520-0477(1998)079<1307:HOCW>2.0.CO;2.

Skamarock, W. C., R. Rotunno, and J. B. Klemp, 1999: Models of coastally trapped disturbances. *J. Atmos. Sci.*, **56**, 3349–3365, doi:10.1175/1520-0469(1999)056<3349:MOCTD>2.0.CO;2.

——, and Coauthors, 2008: A description of the Advanced Research WRF version 3. NCAR Tech. Note NCAR/TN-475+STR, 113 pp. [Available online at http://www.mmm.ucar.edu/wrf/users/docs/arw_v3_bw.pdf.]

Thompson, W. T., T. Haack, J. D. Doyle, and S. D. Burk, 1997: A nonhydrostatic mesoscale simulation of the 10–11 June 1994 coastally trapped wind reversal. *Mon. Wea. Rev.*, **125**, 3211–3230, doi:10.1175/1520-0493(1997)125<3211%3AANMSOT>2.0.CO%3B2.

——, S. D. Burk, and J. Lewis, 2005: Fog and low clouds in a coastally trapped disturbance. *J. Geophys. Res.*, **110**, D18213, doi:10.1029/2004JD005522.

Wang, Z., P. Wechsler, W. Kuestner, J. French, A. R. Rodi, B. Glover, M. Burkhart, and D. Lukens, 2009: Wyoming Cloud Lidar: Instrument description and applications. *Opt. Express*, **17**, 13 576–13 587, doi:10.1364/OE.17.013576.

——, J. French, G. Vali, and P. Wechsler, 2012: Single aircraft integration of remote sensing and in situ sampling for the study of cloud microphysics and dynamics. *Bull. Amer. Meteor. Soc.*, **93**, 653–668, doi:10.1175/BAMS-D-11-00044.1.

Zemba, J., and C. A. Friehe, 1987: The marine boundary layer jet in the Coastal Ocean Dynamics Experiment. *J. Geophys. Res.*, **92**, 1489–1496, doi:10.1029/JC092iC02p01489.